Periodicity in the Auto-correlation as a Mechanism for Regularly Occurring Zero-Crossings or Extreme Values of a Gaussian Process

Lorna R M Wilson*
Institute for Mathematical Innovation, University of Bath, Bath, UK

Keith I Hopcraft
Department of Mathematical Sciences, University of Nottingham, Nottingham, UK
(Dated: October 27, 2017)

The problem of zero-crossings is of great historical prevalence and promises extensive application. The challenge is to establish precisely how the auto-correlation function or power spectrum of a one-dimensional continuous random process determines the density function of the intervals between the zero-crossings of that process. This paper investigates the case where periodicities are incorporated into the auto-correlation function of a smooth process. Numerical simulations, and statistics about the number of crossings in a fixed interval, reveal that in this case the zero-crossings segue between a random and deterministic point process depending on the relative timescales of the periodic and non-periodic components of the auto-correlation function. By considering the Laplace transform of the density function, we show that incorporating correlation between successive intervals is essential to obtaining accurate results for the interval variance. The same method enables prediction of the density function tail in some regions, and we suggest approaches for extending this work to cover all regions. In an ever-more complex world, the potential applications for this scale of regularity in a random process are far reaching and powerful.

I. INTRODUCTION

One-dimensional, continuous random processes are used to model a huge variety of real world phenomena. In particular, the zero-crossings of such processes are relevant to problems such as diffusion [1], signal processing [2], speech analysis [3], fault detection [4], radio waves [5], ocean waves [6, 7], hydrology [8], meteorology [9], genetics [10] and finance [11, 12]. Zero-crossings have also impacted on queuing theory [13], reliability theory [14] and applied probability [15, 16].

Not only do zero-crossings provide information about return times and threshold crossings, but they also tell us about extreme values. This is because the turning points of one random process occur at the same time as the zeros of the derivative of that process.

Blake and Lindsey [17] commented in a review of the zero-crossing problem, that 'the ultimate goal of such an investigation would be to determine the probability density of the lengths of the intervals between zeros of the process' and noted that 'very little success has been achieved in finding this function'. Over forty years on, this is still very much the case. The only analytical result for the density of interval times is particular to a Gaussian process with a specific auto-correlation function [18].

In this paper we consider smooth, Gaussian processes which are fully characterised by the auto-correlation function and straightforward to simulate. We make the auto-correlation function our starting point for investigation, choosing a particular oscillatory form introduced previously in conference proceedings [19], and motivated in the next section. Statistics for the number of zero-crossings occurring within a set time period are calculated and verified by simulations of the process. These demonstrate that such periodicities in the auto-correlation function describe a process for which the zero-crossings segue between a random and deterministic point process - this is a novel result with great potential for application. We extend the work of McFadden [20, 21] to describe the interval variance and density function in this particular case. We present new results and explore the limitations of these methods.

The interplay between randomness and order is a pervasive component of the dialogue around of complex systems; it is present in the type of exploratory behaviour observed by ants [22], or the development of the circulatory and nervous systems [23, 24]. The precise way in which components interact both randomly and deterministically determines the emergent behaviour of the system as a whole. This balancing act between random exploration and deterministic exploitation has been hypothesised to be a general property of intelligent, adaptive systems [25]. Furthermore, continuous one-dimensional random processes are often an effective way to build randomness, whatever its origin, into a model. Their most established application is in signal processing, and much of the mathematical theory was developed with this in mind. Real-world continuous processes frequently prove difficult to measure and analyse in full, and it can be informative to observe only their crossings, reducing them to a series of points in time, or a point process. By linking a continuous Gaussian process to a random point process, the regularity of which is directly determined by the auto-correlation function, the work of this paper presents a novel and valuable modelling tool.

* l.wilson@bath.ac.uk

II. PERIODICITY AND THE AUTO-CORRELATION FUNCTION

The auto-correlation function (or the corresponding power spectrum) describes the memory of the process and is essential to the determination of the statistical properties of the process and its zero-crossings. For a stationary process $X(\tau)$ with zero mean, the auto-correlation function is independent of the origin of time and given by

$$\rho(\tau') = \frac{\langle X(0)X(\tau')\rangle}{\sigma^2}.$$

where σ^2 is the variance of the process. It is a real valued function satisfying $|\rho(\tau')| \leq \rho(0)\ \forall\tau'$ with $\rho(0) = 1$ and as $\tau' \to \infty$, $\rho(\tau') \to 0$. Due to the stationarity of the process $X(\tau)$, $\rho(\tau')$ is symmetric about the origin. Finally, the power spectrum of the correlation model, which describes how the variance of $X(t)$ is distributed over its frequency components, must be positive definite. The power spectrum $\bar{\rho}(\omega)$ is given by Wiener-Khinchin Theorem [26–28] as the Fourier transform of $\rho(\tau)$;

$$\bar{\rho}(\omega) = 2\int_0^\infty \rho(t)\cos(2\pi\omega t)\mathrm{d}t. \tag{1}$$

When prescribing an auto-correlation function it must satisfy all of these properties and so the power spectrum may place constraints on the allowable values of any parameters of $\rho(\tau)$.

For the mean rate of zero-crossings to exist, the auto-correlation function must be twice differentiable at the origin i.e. $\rho(\tau) = 1 - b\tau^2 + O(\tau^{2+\mu})$ with $b, \mu > 0$. If this is not the case then the auto-correlation describes a fractal process, where an infinite number of zeros-crossings fails to be resolved by magnification [29]. Where this is the case, and $0 < \mu < 2$, the resulting process is known as sub-fractal. This is because the mean rate of zero-crossings of the process itself exists, but the mean rate does not exist for the differentiated process which exhibits fractal behaviour. In the case where $\mu = 2$, the process is smooth and all derivatives exist. It is these smooth processes with which this paper is concerned.

In order to motivate the precise form of auto-correlation we have chosen to investigate, we first consider the signal $S(t)$ formed by a Gaussian process $G(t)$, modulated by a cosinusoidal wave with a random phase shift. The signal exhibits interplay between the random behaviour of $G(t)$ and deterministic, periodic behaviour governed by the cosine. Zeros resulting from the random process break up the regular crossings of the cosine.

We define the signal is $S(t)$:

$$S(t) := \sqrt{2}\cos(at + \phi_0)G(t). \tag{2}$$

where $\phi_0 \sim \mathrm{U}(0, 2\pi)$ is uniformly distributed random phase fixed in time, and $G(t)$ is an independent, stationary Gaussian process with zero mean, unit variance and auto-correlation function $g(\tau) = \langle G(0)G(\tau)\rangle$. A realisation of $S(t)$ and $G(t)$ is shown in Figure 1.

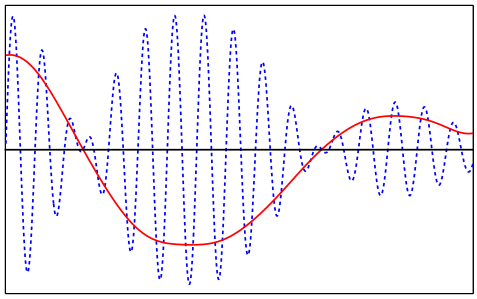

Figure 1. A representation of $G(t)$ (solid line) and $S(t)$ (dotted line)

The auto-correlation function of the signal $S(t)$ is

$$\begin{aligned}\rho_s(\tau) &= \frac{\langle S(0)S(\tau)\rangle}{\sigma_s^2} \\ &= \frac{2\langle\cos(\phi_0)G(0)\cos(a\tau+\phi_0)G(\tau)\rangle}{\sigma_s^2}.\end{aligned}$$

Due to the independence of $G(t)$ and the cosine, the variance of $S(t)$ is 1. Therefore

$$\begin{aligned}\rho_s(\tau) &= 2\langle\cos(\phi_0)G(0)\cos(a\tau+\phi_0)G(\tau)\rangle \\ &= 2\langle\cos(\phi_0)\cos(a\tau+\phi_0)\rangle\langle G(0)G(\tau)\rangle \\ &= \cos(a\tau)\, g(\tau).\end{aligned}$$

The auto-correlation function $g(\tau)$ determines the behaviour of the random process $G(t)$. For a smooth, twice-differentiable process a suitable choice of auto-correlation function is

$$g(\tau) = \left(1 + \frac{\tau^2}{\gamma}\right)^{-\gamma/2}$$

where γ determines the rate of decay of the memory of the process.

In this paper we consider the Gaussian process $X(t)$ with zero mean, unit variance and the same auto-correlation function as $S(t)$:

$$\rho(\tau) = \cos(a\tau)\left(1 + \frac{\tau^2}{\gamma}\right).^{-\gamma/2} \tag{3}$$

The process will only be considered for $\gamma \geq 2$ where numerical analysis reveals that the power spectrum is positive definite for all values of a.

It should be noted that, while it has the same mean and variance as $X(t)$, the signal $S(t)$ is not a Gaussian process. The PDF of S is:

$$p(S) = \frac{1}{2\pi^{3/2}}K_0\left(\frac{S^2}{8}\right)\exp\left(-\frac{S^2}{8}\right)$$

where K_0 is a modified Bessel function of the second kind [30]. This expression for the PDF of S has a logarithmic

singularity at the origin, meaning $S(t)$ spends more time near the origin than the Gaussian process $X(t)$.

To sumarise: $G(t)$ is a Gaussian process with zero mean, unit variance, and auto-correlation $g(\tau)$. $S(t)$ is the non Gaussian random process obtained by modulating $G(t)$ with a cosine, it also has zero mean and unit variance. $X(t)$ is a Gaussian process with zero mean, unit variance and the same oscillatory auto-correlation function as $S(t)$.

A. Timescales

The auto-correlation function (3) has two timescales: $\ell_1 = 1/a$ from the cosine, and ℓ_2 from the power-law. The power-law governs the overall decay of the auto-correlation function. The 'width' of this power-law reflects the overall memory of the corresponding Gaussian process, it is this that the timescale ℓ_2 should capture. In the limit $\gamma \to \infty$, the power law is a Gaussian function:

$$\lim_{\gamma\to\infty}\left(1+\frac{\tau^2}{\gamma}\right)^{-\gamma/2} = \exp\left(-\frac{\tau^2}{2}\right)$$

for which the obvious choice for the timescale is $\ell_2 = \sqrt{2}$.

The 'width' of the power-law is compared to that of the Gaussian function as follows: With argument $\tau = \sqrt{2}$, the Gaussian function is e^{-1} and this is set to be equivalent to the power law with argument ℓ_2 ,

$$\left(1+\frac{(\ell_2)^2}{\gamma}\right)^{-\gamma/2} = e^{-1}$$

it then follows that

$$\ell_2 = \left(\gamma e^{2/\gamma} - \gamma\right)^{\frac{1}{2}}. \tag{4}$$

This has the properties that $\ell_2 \to \sqrt{2}$ as $\gamma \to \infty$ and $\ell_2 \to \infty$ as $\gamma \to 0$.

It should be noted that there are alternative ways to characterise the 'width' of the (symmetric) power-law function. For example taking a scalar multiplier of the (positive) square root of the variance of the power-law. The scalar multiplier can be set so that the property $\ell_2 \to \sqrt{2}$ as $\gamma \to \infty$ is preserved, however $\ell_2 \to \infty$ as $\gamma \to 3$, which may be problematic as the Gaussian process is considered for $\gamma \geq 2$. Another alternative is mean value of the power-law over the positive real line. Again, the scalar multiplier can be chosen to preserve the property $\ell_2 \to \sqrt{2}$ as $\gamma \to \infty$. In this case $\ell_2 \to \infty 2$ as $\gamma \to 2$.

All these possible timescales for the power-law function are monotonically decreasing, converge to $\sqrt{2}$ as $\gamma \to \infty$, and diverge for small values of γ. For the purposes of this paper, this is sufficient information about $_2$ to aid explanation of the trends observed in the corresponding Gaussian process. Further analysis of this function will require careful justification of timescales used.

B. Mean Crossing Rate

A zero-crossing is a sign change of a process from positive to negative values or vice versa. The mean zero-crossing rate is the expected number of zero-crossings per unit time. For the Gaussian process $X(t)$, the mean rate of crossings $\bar{r}$, depends only on the second derivative of the auto-correlation function at the origin. It is calculated via the well known result first presented in section 3.3 of Rice's report on 'Mathematical Analysis of Random Noise' [31]:

$$\bar{r} = \frac{\left(-\rho''(0)\right)^{1/2}}{\pi} = \frac{(1+a^2)^{1/2}}{\pi}. \tag{5}$$

Note that the mean rate of crossings is independent of γ. As the auto-correlation function gets more oscillatory with increasing a,the rate of zero-crossings increases.

The mean rate of crossings for the signal $S(t)$ is

$$\bar{r}_s = \frac{a}{\pi} + \bar{r}_g = \frac{1+a}{\pi}.$$

In the limits $a \to 0$ and $a \to \infty$, the mean rate of zero-crossings of the signal $S(t)$ and the Gaussian process $X(t)$ are the same.

C. Fano Factor

The fluctuations in the number N of zero-crossings, in an interval of fixed length T, are described by the Fano Factor [32]:

$$F(T) := \frac{\mathrm{Var}(N)}{\langle N\rangle} = 1 + \frac{\langle N(N-1)\rangle}{\langle N\rangle} - \langle N\rangle.$$

The Fano factor is the discrete analogue of the coefficient of variation: it quantifies the departure of the fluctuations in random events occurring in a window of length T from purely Poisson statistics. It was first used in particle detection to detect deviations in dispersion of the number of ions produced by constant amounts of radiation energy. It has proved useful for characterising neural spiking [33] and is extensively used in photonics [34]. When there are Poisson number fluctuations, $\mathrm{Var}(N) = \langle N\rangle$ and $F(T) = 1$. If fluctuations are super-Poissonian then zeros occur in clusters and $F > 1$. In the case of sub-Poissonian behaviour where zeros are repelled from each other, $F < 1$.

The Fano Factor is calculated via Rice's result for the mean number of crossings (5) and the following result by Steinberg et al. [35]:

$$\langle N(N-1)\rangle = \frac{2T^2}{\pi^2}\int_0^1 \frac{\mathrm{d}y(1-y)}{\left(1-\rho^2(yT)\right)^{3/2}} \left[|A^2-B^2|^{1/2} + B\arctan\left(\frac{B}{|A^2-B^2|^{1/2}}\right)\right]$$

$$\text{where}\quad A = -\rho''(0)\left[1-\rho^2(yT)\right] - \rho'^2(yT)$$

$$\text{and}\quad B = \rho''(yT)\left[1-\rho^2(yT)\right] + \rho(yT)\rho'^2(yT) \tag{6}$$

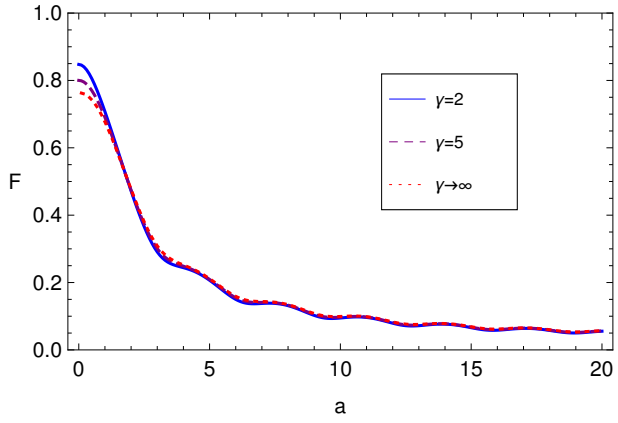

(a) $T = 1$

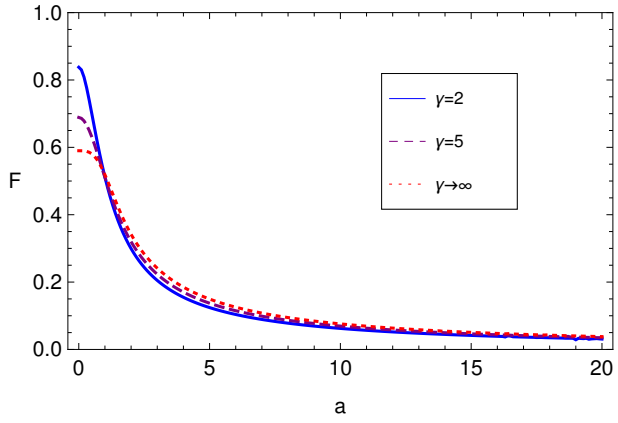

(b) T=10

Figure 2. Fano Factor as a function of a with $\gamma = 2$, $\gamma = 5$ and $\gamma \to \infty$

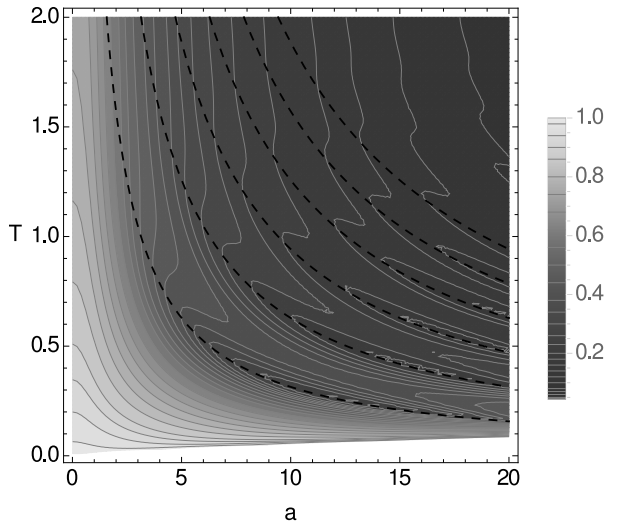

Figure 3. F parametrised against a, and the integration time T. The dashed lines show $T = n\langle\tau\rangle$ for $n = 1...6$.

The cases $\gamma = 2$, $\gamma = 5$ and $\gamma \to \infty$ are compared in Figure 2 for $T = 1$ and $T = 10$. The overriding trend is that as a increases, the Fano Factor decreases. For large a (i.e. when $\ell_1 \ll \ell_2$) the cosine in the auto-correlation function oscillates much faster than the power-law decays. The result is that the effect of the cosine dominates the behaviour of the process; there is little fluctuation in the number of zero-crossings in an interval, i.e. zeros occur at more regular intervals and the process appears increasingly 'deterministic'.

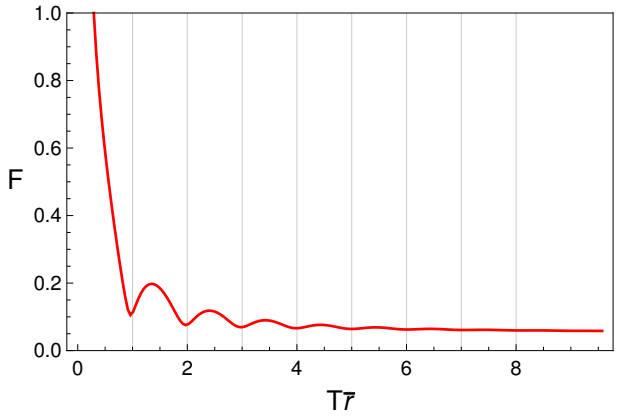

Figure 4. F for $a = 15$ and $\gamma \to \infty$, plotted against $T\bar{r}$ so that the integer-valued gridlines correspond to $T = n\langle\tau\rangle$ for $n = 1...8$.

This is reflective of the interplay between the random behaviour of $G(t)$ and deterministic, periodic behaviour governed by the cosine in signal $S(t)$. For small enough a, when the power-law dominates the auto-correlation function, F increases with decreasing γ. When a is large enough that the oscillations in the auto-correlation function significantly affect the process, this effect is reversed and F decreases with decreasing γ. The greater the difference $\ell_1 \ll \ell_2$, the more the cosine affects the process and the more regular the zero-crossings are.

For smaller values of T there are ripples in $F(a)$, this rich behaviour of the Fano factor is displayed in Figure 3. In order to understand how these ripples in the Fano Factor relate to the behaviour of $X(t)$ itself, we consider F as a function of T as in Figure 4, which reveals that the first local minimum of F occurs when the fixed interval length T is equal to the mean interval between zero-crossings, i.e. $T = 1/\bar{r}$. Subsequent local minima occur at $T = n/\bar{r}$ (where n take integer values) until, with sufficiently large T, the ripples are damped. Zero-crossings occur regularly for large enough a and so, when $T = n/\bar{r}$ there is very little fluctuation in the number of zeros which is highly likely to be n, but when $T = (n+1)/2\bar{r}$ there are equally likely to be n or $n+1$ zeros in an interval. This change in fluctuation in the number of zeros means that F is locally larger when $T = (n+1)/2$ and smaller when $T = n/\bar{r}$. This is plainly visibly in Figure 4 where the grid-lines at n correspond to the minima in F.

III. SIMULATION RESULTS

Simulations are obtained by Fourier transforming both Gaussian random noise and the auto-correlation function, then multiplying them in the frequency domain and Fourier inverting the result back into 'real' space (this is equivalent to forming a convolution of Gaussian random noise and the auto-correlation function). This is an established method covered in many texts [28].

A. Variance of the Intervals

Figure 5 shows simulations of the variance of the interval between successive zero-crossings, for $\gamma \to \infty, \gamma = 5$ and $\gamma = 2$ in the auto-correlation function

$$\rho(\tau) = \cos(a\tau)\left(1 + \frac{\tau^2}{\gamma}\right)^{-\gamma/2}.$$

The variance declines rapidly with increasing a, and becomes less than the mean at $a \sim 1.2$, indicating the distribution for the intervals is narrowing. The effect of γ, or equivalently the size of the power-law timescale ℓ_2, is minimal. A larger ℓ_2 will result in the power-law dominating the behaviour of the process until a larger cosine timescale $\ell_1 = 1/a$ (equivalent to a smaller value of a) is attained. In the region where the power-law dominates the behaviour of the process, a larger ℓ_2 results in a higher variance. In the region where the cosine dominates the process, the zero-crossings occur more regularly and the variance is small, and the effect of ℓ_2 negligible.

The remainder of this paper will focus on the Gaussian limit case where $\gamma \to \infty$ (or $\ell_2 \to 0$)such that

$$\rho(\tau) = \cos(a\tau)\exp\left(-\frac{\tau^2}{2}\right)$$

and $\ell_2 = \sqrt{2}$. Here, a relatively small cosine timescale ℓ_1 results in the Gaussian function dominating the behaviour so that intervals have a greater variance. For ℓ_1 small enough the process will behave as if it has only a Gaussian auto-crorrelation functions have been used to represent physical processes such as the scattering of light from a random-phase-changing screen [36]. A large cosine timescale ℓ_1 means the cosine dominates the behaviour of the process, resulting in low interval variance and regular zero-crossings. This could be representative of processes that exhibit some periodicity, such as the nearly periodic 11-year solar sunspot cycle [37].

B. Density Function of the Intervals

The time between zero-crossing events is a *continuous* random variable τ with $P_n(\tau)\mathrm{d}\tau$ denoting the probability that the $(n+1)$th event occurring after time t_0 falls within the interval $t_0 + \tau$ to $t_0 + \tau + \mathrm{d}\tau$ and $P_0(\tau)$ is the

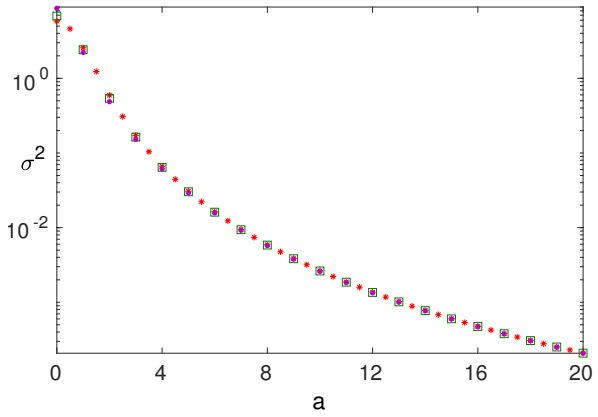

Figure 5. Simulation results for the variance of the intervals. For $\gamma \to \infty$ (+), $\gamma = 5$ (□) and $\gamma = 2$ (X).

density of the interval length between successive events. Figure 6 shows three plots of simulations of the inter-event density function $P_0(\tau)$. Figure 6a shows $P_0(\tau)$ for values of a from 0 to 20. As a increases, the mean decreases and the PDF shifts to smaller values of τ in accordance with (5). In addition, the PDF becomes more concentrated around the mean, reflecting the greater regularity of the zero-crossings. This is better observed in the Figure 6b, which shows the re-normalised PDF plotted on the rescaled axis $\tau/\langle\tau\rangle$. The previous sections showed that, with increasing a, successive intervals become highly correlated i.e $\kappa \to 1$ and $\sigma^2 \to 0$ as $a \to \infty$. These simulation results confirm that the corresponding effect on the PDF is that $P_0(\tau)$ tends towards a delta-function located at the mean interval spacing $\tau = \langle\tau\rangle$.

Figure 6c contains the same data as 6b one, but with a logarithmic scale on the y-axis. This gives a clear representation of the tail of the PDF. When $a = 0$, the tail is a straight line corresponding to exponential decay. For higher values of a there is a shoulder in the tail at around twice the mean. We consider the possibility that this shoulder is an artefact of simulation whereby two crossings appear within one time-step so that a longer interval is falsely recorded. This is done by comparing the PDF simulated with the resolution used throughout this paper, and at twice that resolution. In Figure 7 it can be seen that shoulder is almost identical in both cases. The simulations of the smooth process $X(t)$ are of high enough resolution that miss-recording zero-crossings, that are distinct at the order of magnification of one time-step, has no perceptible impact on the resulting density function. The explanation is then, that occasionally the process turns when it is very close to zero, resulting in a zero-crossing interval of approximately twice the mean length. It is important to note that this 'touch' of the zero line occurs very infrequently and is only perceptible on the logarithmic scale plots.

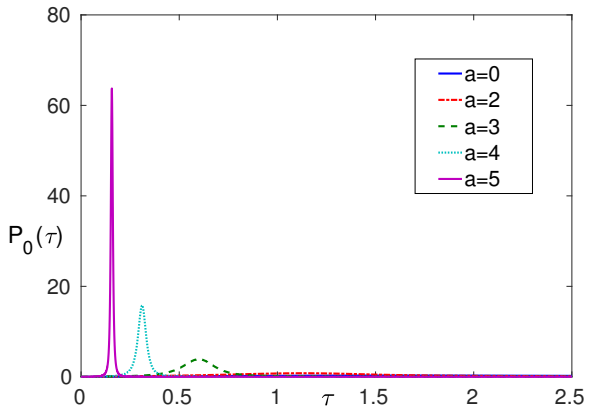

(a) $P_0(\tau)$ for $a = 0, 2, 5, 10, 20$.

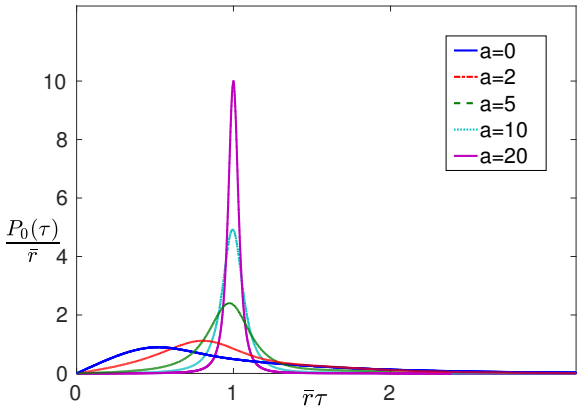

(b) $P_0(\tau)$ for $a = 0, 2, 5, 10, 20$, plotted against $\bar{r}\tau$.

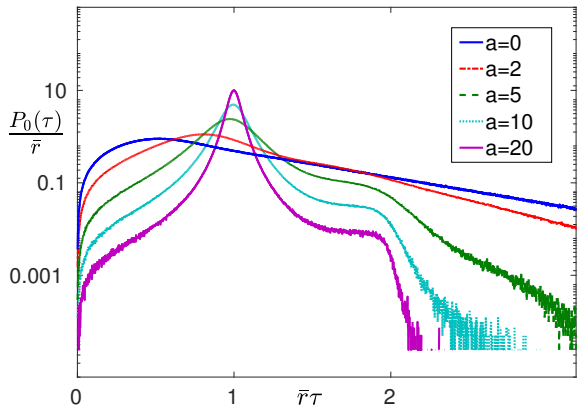

(c) Re-normalised simulations of $P_0(\tau)$ for $a = 0, 2, 5, 10, 20$, plotted on a logarithmic axes against $\bar{r}\tau$.

Figure 6. Simulations of the interval density function $P_0(\tau)$.

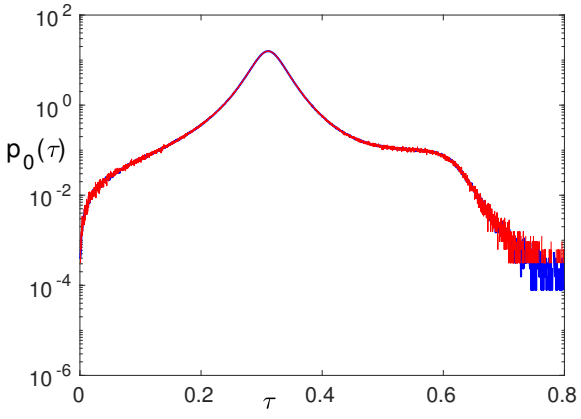

Figure 7. Simulations of PDF for $a = 10$ with the resolution used throughout this paper (red dashed), and at twice this resolution (blue solid).

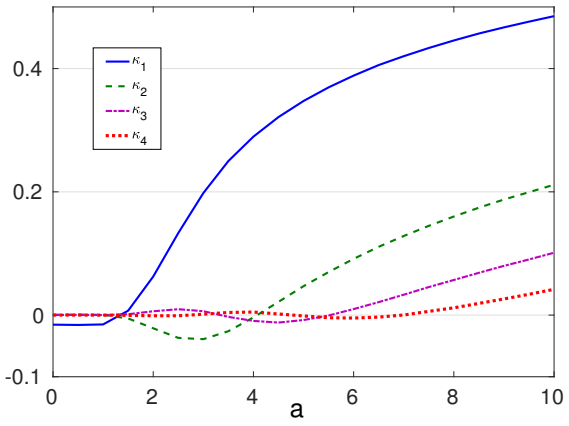

Figure 8. The simulated values of the correlation coefficients (7).

C. Correlations Between the Intervals

The correlation coefficient describes the correlation between the ith and $(i+j)$th intervals, τ_i and τ_{i+j}, and is defined as

$$\kappa_j = \frac{\langle \tau_i \tau_{i+j} \rangle - \langle \tau \rangle^2}{\sigma^2} \qquad j > 0.$$

When intervals are independent of each other, they are uncorrelated and $\kappa_j = 0$. When $\kappa_j > 0$, intervals are positively correlated with $\kappa_j = 1$ corresponding to full correlation where the ith and $(i+j)$th intervals are the same length. When $\kappa_j < 0$, intervals are negatively correlated so that if the ith interval is long, the $(i+j)$th interval is likely to be short.

Figure 8 shows the simulated results for the correlation coefficients κ_1 to κ_4. The graph of κ_1 is negative for small a, showing that successive interval lengths are anti-correlated in this region. This indicates that zeros

of the random process are repelled from each other where they are principally affected by the exponential factor in $\rho(\tau)$, $g(\tau) = \exp(-\tau^2/2)$. This is because the process is smooth and, unlike a fractal or sub-fractal process, cannot change sign or slope in an arbitrary short time. The intervals become positively correlated once the oscillations in $\rho(\tau)$ begin to occur within the characteristic width of the exponential function (i.e. for $\ell_1 < \ell_2$). This demonstrates that the process is becoming more regular, in accord with the behaviour found for $F(T)$ in section II C.

The higher order correlation coefficients κ_2, κ_3 and κ_4 all start very close to zero. With progressively increasing a they then oscillate close to zero, through periods of correlation and anti-correlation, before becoming positive and strictly increasing. The number of oscillations observed corresponds to the order of the correlation coefficient, i.e. κ_2 crossed the axis twice and κ_4 crosses 4 times. This structure comes about through the interplay of the time-scales of the cosine ℓ_1 and of the power-law ℓ_2, described in section III A. In the limit $\ell_1 \to 0$ all the $\kappa_i \to 1$, indicating a trend towards exact periodicity and determinism. These simulation results demonstrate that intervals between zero-crossings are not independent of each other.

IV. CALCULATING THE INTERVAL VARIANCE

In this section we present McFadden's derivation of two expressions for the variance under the assumption that successive intervals are independent. The simulation results presented in the previous section demonstrate that the independent intervals assumption is not correct. We extend the work of McFadden to consider two possible assumptions for the structure of interval correlation. Again, we obtain expressions for the variance. In all three cases, the derivation of the expressions for the variance begins with some exact results: two infinite sums. The different assumtions about correlations are then substituted in and result in polynomials in laplace transform of $P_n(t)$. The second moment in the expansion of this Laplace transform is then identified so that expressions for the variance can be determined and numerically evaluated.

1. Exact Results

Recall from section III B that $P_n(\tau)$ is the density of the interval length between $n+1$ successive events. Two infinite series of $P_n(\tau)$ were derived by McFadden [21].

The first relates to the clipped process of $X(t)$, which identifies the locations of the zero-crossings, and is defined as:

$$\xi(t) = \begin{cases} 1 & X(t) \geq 0 \\ -1 & X(t) < 0 \end{cases}$$

The auto-correlation function of $\xi(t)$ is $R(\tau') = \langle \xi(t)\xi(t+\tau') \rangle$, from which it can be shown that

$$\frac{R''(\tau)}{4\bar{r}} = \sum_{n=0}^{\infty} (-1)^n P_n(\tau). \tag{7}$$

where $\bar{r}$ is the crossing rate (5).

McFadden derived a second infinite series relating $P_n(\tau)$ to $U(\tau)$ where $U(\tau)\mathrm{d}\tau$ is defined to be the conditional probability that a zero occurs in the interval $(t+\tau, t+\tau+\mathrm{d}\tau)$, given one occurs at t. If there is a zero in the interval $(t+\tau, t+\tau+\mathrm{d}\tau)$, it must be either the 1st, 2nd,3rd.... up to infinity and hence:

$$U(\tau) = \sum_{n=0}^{\infty} P_n(\tau). \tag{8}$$

Deriving equations for the variance of the zero-crossing intervals requires the following Laplace transform:

$$u(s) = \mathcal{L}\left((U(\tau)\right) \tag{9}$$

$$r(s) = \mathcal{L}\left(\frac{R''(\tau)}{4\bar{r}}\right) \tag{10}$$

$$p_n(s) = \mathcal{L}\left(P_n(\tau)\right) \tag{11}$$

so that the infinite sums can be expressed as

$$r(s) = \sum_{n=0}^{\infty} (-1)^n p_n(s) \tag{12}$$

$$u(s) = \sum_{n=0}^{\infty} p_n(s). \tag{13}$$

Both these infinite sums, expressed in $P_n(\tau)$ or $p_n(s)$, are *exact results* for a general, symmetric, stationary, ergodic process, meaning any sample from the process must represent the average statistical properties of the entire process.

A. Assumption: Independent Intervals

Making the *assumption* that successive intervals between zero-crossings are statistically independent the the interval sums are given by convolutions of $P_0(t)$, or in terms of the Laplace transforms:

$$p_n(s) = p_0(s)^{n+1}. \tag{14}$$

Substituting this into the infinite sums (12) and (13) obtains two independent equations for $p_0(s)$:

$$p_0(s) = \frac{r(s)}{1 - r(s)} \tag{15}$$

$$p_0(s) = \frac{u(s)}{1 + u(s)} \tag{16}$$

From the definition of the Laplace transform we obtain the moments of $P_0(\tau)$ from derivatives of $p_0(s)$ at $s = 0$.

By matching coefficients of equal powers of s in the expansion of (15), expressions for $\langle\tau\rangle$ and $\langle\tau^2\rangle$ are obtained. The resulting expression for the variance is then:

$$\sigma_I^2 = \frac{2I}{\bar{r}}.$$

with I defined as the integral

$$I = \int_0^\infty R(\tau)\mathrm{d}\tau.$$

The function $u(s)$ cannot be expanded about the origin but the transform $v(s) = u(s) - \bar{r}/s$ enables expansions of $p_0(s)$ and $v(s)$ to be substituted into equation (16). We then obtain a second expression for the variance through matching powers of s:

$$\sigma_J^2 = \frac{1 + 2J}{\bar{r}^2}$$

where

$$J = \int_0^\infty [U(\tau) - \bar{r}]\mathrm{d}\tau.$$

The evaluation of the integrals I and J depend on the precise distribution of the process. They two expressions for the variance, σ_I and σ_J could be expected to match if, and only if, the assumption of statistical independence of intervals were correct.

1. *Numerical Evaluation*

Evaluating the clipped auto-correlation function requires an integral of the bivariate density function for the process $X(t)$. The result for a Gaussian process is given by the van-Vleck theorem [38]:

$$R(\tau) = \frac{2}{\pi}\arcsin\left(\rho(\tau)\right). \tag{17}$$

For a Gaussian process, the function $U(\tau)$ has been determined by Rice [31] (sectiion 3.4) to be,

$$U(\tau) = \frac{1}{\bar{r}\pi^2\left(1-\rho^2(\tau)\right)^{3/2}} \left[|A^2 - B^2|^{1/2} + B\arctan\left(\frac{B}{|A^2-B^2|^{1/2}}\right)\right]$$

with A and B given in (6). These permit σ_I^2 and σ_J^2 to be evaluated by quadrature.

In Figure 9 numerical evaluations of the variance in both cases are compared to results from simulations. Both σ_I^2 and σ_J^2 display the same overall behaviour as the simulated variance with slight over or underestimation of a similar magnitude. The findings of the previous sections are affirmed, with the decreasing variance reflecting increasingly regular zero-crossings.

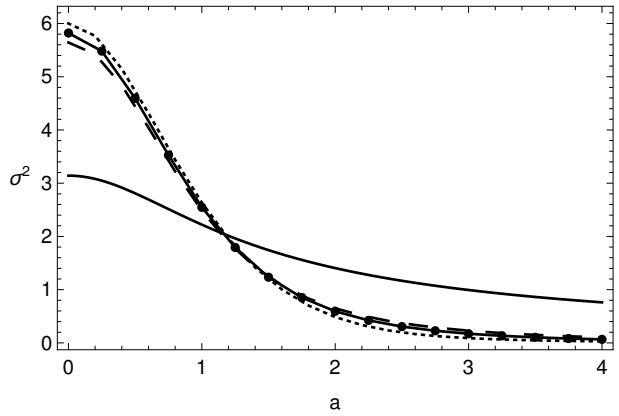

Figure 9. The variance from simulations (circles) and numerical evaluation of the model σ_I^2 from (IV A) (dotted) and σ_J^2 from (IV A) (dashed) as well as the mean interval length via (5) (solid)

The difference between the two results for the variance, although small, implies that intervals between zero-crossings are not independent of each other. At $a \sim 1.3$, $\sigma_I^2 = \sigma_J^2$, suggesting that the intervals may be uncorrelated at this point, however simulation results show this is not the case at this point does *not* correspond to $\kappa_j = 0$. We conclude that incorporating interval correlation is necessary.

B. Assumption: Interval Correlation

A strategy for relaxing the assumption of statistical independence was suggested by McFadden [21] through the introduction of the undetermined function $a_n(s)$ into the assumed model so that:

$$p_n(s) = a_n(s)p_0^{n+1}(s). \tag{18}$$

This relation is a generalization of 14, which followed when successive intervals were assumed to be independent of each other. The function $a_n(s)$ embodies information about correlation. As with the uncorrelated case, this relation will be substituted into the two infinite sums 12 and 13, and the second moment in the expansion of $p_0(s)$ will be identified so that two expressions for the variance can be found. UNlike the uncorrelated case, the extra degree of freedom introduced by $a_n(s)$ will enable these two expressions for the variance to be equated to each other. First, $a_n(s)$ must be determined.

It is possible to determine $a_n(s)$ using the fact that $p_n(s)$ is a moment generating function with expansion near the origin

$$p_n(s) = 1 - \langle T\rangle s + \langle T^2\rangle s^2 + O(s^4)$$

where

$$T = \sum_{j=1}^{n+1}\tau_j.$$

Noting that $\langle T\rangle = (n+1)\langle\tau\rangle$ the expansion for $a_n(s)$ follows

$$a_n(s) = \frac{p_n(s)}{p_0(s)^{n+1}}$$
$$= 1 + \frac{s^2}{2}\left(\langle T^2\rangle - (n+1)\left(n\langle\tau\rangle^2 + \langle\tau^2\rangle\right)\right) + O(s^4).$$

The quantity $\langle T^2\rangle$ contains terms of the form $\langle\tau_i\tau_j\rangle$ and so, in order to evaluate these terms the correlation coefficient (7) is required. Then

$$\langle T^2\rangle = \left\langle\left(\sum_{i=1}^{n+1}\tau_i\right)^2\right\rangle = \left\langle\sum_{i=1}^{n+1}\tau_i\sum_{j=1}^{n+1}\tau_j\right\rangle$$
$$= 2\sum_{j=1}^{n}(n-j+1)\langle\tau_i\tau_{i+j}\rangle + (n+1)\langle\tau^2\rangle$$
$$= 2\sigma^2\sum_{j=1}^{n}(n-j+1)\kappa_j + n(n+1)\langle\tau\rangle^2 + (n+1)\langle\tau^2\rangle$$

Combining these results yields the simpler form:

$$a_n(s) = 1 + s^2\sigma^2\sum_{j=1}^{n}(n-j+1)\kappa_j \qquad n>0 \quad (19)$$
$$a_0(s) = 1. \quad (20)$$

Obtaining a closed form expression (involving only $\kappa = \kappa_1$) for $a_n(s)$ requires a suitable closure model for the κ_j's. In this paper we explore two: a Markov chain model, and a truncated model.

1. Markov Chain Correlation Model

McFadden made the *assumption* that the intervals form a Markov chain yielding the closure condition $\kappa_j = \kappa^j$, where $\kappa = \kappa_1$, the correlation coefficient for consecutive intervals. Our simulation results in Figure 8 suggest this is an appropriate model for large enough a.

Substituting the Markov chain closure condition into (19) yields

$$a_n(s) = 1 + \frac{s^2\sigma^2\kappa}{(1-\kappa)^2}\left(n - (n+1)\kappa + \kappa^{n+1}\right) + O(s^3). \quad (21)$$

This enables the evaluation of (18) in the infinite sums (12) and (13). In the uncorrelated, independent intervals, case this resulted in two quadratic equations (15) and (16), the additional information about interval correlation contained in (21) results in the following cubic equations in $p_0(s)$:

$$r(s) = \frac{p_0}{1+p_0} - \frac{\kappa(\sigma s p_0)^2}{(1+p_0)^2(1+\kappa p_0)} \quad (22)$$
$$u(s) = \frac{p_0}{1-p_0} + \frac{\kappa(\sigma s p_0)^2}{(1-p_0)^2(1-\kappa p_0)} \quad (23)$$

which reduce to the uncorrelated case (15-16) when $\kappa = 0$.

By matching coefficients of equal powers up to $O(s^2)$ in (12) and (22) we obtain

$$\sigma_I^2 = \beta\left(\frac{1+\kappa}{1-\kappa}\right)$$

with

$$\beta = \frac{2I}{\bar{r}}.$$

Though doing so in (13)and (23), via the transform $v(s) = u(s) - \bar{r}/s$, we obtain a second expression for the variance

$$\sigma_J^2 = \frac{\beta}{\alpha^2}\left(\frac{1-\kappa}{1+\kappa}\right)$$

with

$$\alpha = \left(\frac{2\bar{r}I}{1+2J}\right)^{\frac{1}{2}}.$$

The condition that $\sigma_I = \sigma_J > 0$ determines

$$\kappa = \frac{1-\alpha}{1+\alpha} \quad \text{and} \quad \sigma^2 = \frac{\beta}{\alpha}. \quad (24)$$

Figure 10 shows numerical evaluation of the variance and correlation coefficient in (24) plotted against results from simulations. In the case of the variance, the model gives an accurate result, verifying that the theory is effective up to $O(s^2)$ and computation of the integrals in equation (24) are correct. The result for κ is good for small a, it then deviates slightly from the simulated results for $2 < a < 5$. This is the region where simulation results in Figure 8 show that κ_2 or κ_3 are negative, whereas the Markov chain assumption has them as a power of κ_1 and which is positive in this region. For larger a the model appears to reflect simulated results in Figure 8 again as only higher index κ_j's would be negative and their effect is smaller given that all the lower index κ_j's do appear to fit the model.

2. Asymptotic Behaviour of Variance and Correlation Coefficient Under Markov Chain Model

For large enough a, both the variance and the correlation coefficient (24) are described by a power-law. This follows from numerical results which show that

$$\beta \sim \frac{8}{a^4} \qquad \text{and} \qquad \alpha \sim \left(\frac{8}{7a}\right)^{1/2}$$

as $a \to \infty$. Hence

$$\sigma^2 = \frac{\beta}{\alpha} \sim \left(\frac{56}{a^7}\right)^{1/2} \quad (25)$$

and

$$\kappa = \frac{1-\alpha}{1+\alpha} \sim \frac{1-\left(\frac{8}{7a}\right)^{1/2}}{1+\left(\frac{8}{7a}\right)^{1/2}} \tag{26}$$

as $a \to \infty$. Plots of these asymptotic results for σ^2 and κ are shown in Figure 10.

The power-law decay of the interval variance and correlation demonstrates that the dynamics at play in this system are far from simple. On first glance, the variance in Figure 10 might appear to decay exponentially or, like the auto-correlation function, according to a Gaussian function $\exp(-a^2)$. This is not the case, and the effect of the cosine term in the auto-correlation function is bound up in the intricacies resulting from non standard oscillatory integrals.

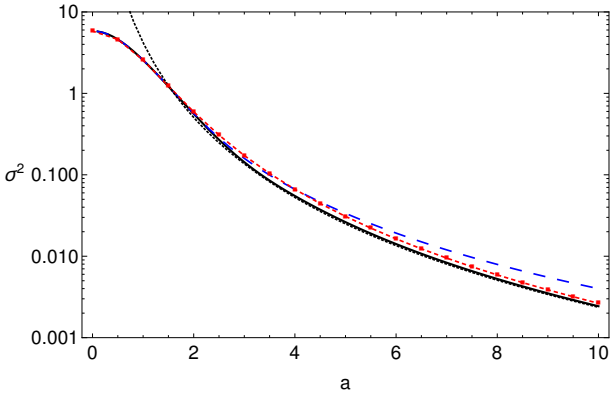

(a) The variance of interval between crossings.

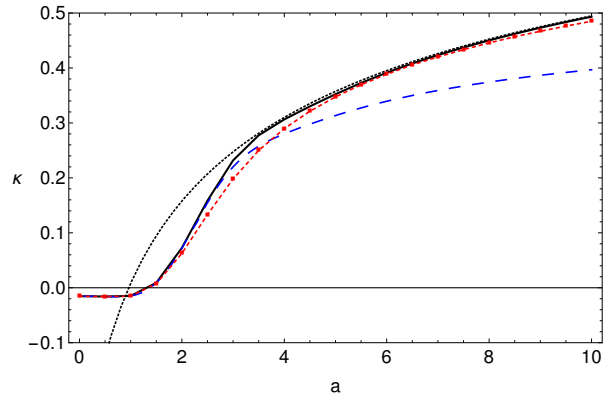

(b) The interval correlation coefficient.

Figure 10. The variance and first order correlation coefficient of the interval between crossings as a function of a: from simulations (squares), from numerical analysis of the Markov chain model (24) (solid) and it's asymptotic limit (25) (dotted), and from numerical analysis of the truncated model (30) (dashed).

3. *Truncated Correlation Model*

The simulation results in Figure 8 show that, while the correlation coefficients do appear to form a Markov chain for large a, this is not an appropriate assumption for an intermediate regime in a. Therefore we propose the equally tractable *assumtion* that only successive intervals are correlated. That is $\kappa_j = 0$ for $j \geq 2$, which gives

$$a_n(s) = 1 + n\sigma^2 s^2 \kappa + O(s^3), \tag{27}$$

whereupon, inserting this and (18) into the infinite sums (12-13) yields quadratic equations for $p_0(s)$

$$r(s) = \frac{p_0}{1+p_0} - \frac{\kappa(\sigma s p_0)^2}{(1+p_0)^2} \tag{28}$$

$$u(s) = \frac{p_0}{1-p_0} + \frac{\kappa(\sigma s p_0)^2}{(1-p_0)^2} \tag{29}$$

which reduce to the uncorrelated result (15-16) when $\kappa = 0$.

Following the same methods as before,

$$\sigma^2 = \frac{1}{2}\left(\beta + \frac{\beta}{\alpha^2}\right), \quad \text{and} \quad \kappa = \frac{1}{2}\left(\frac{1-\alpha^2}{1+\alpha^2}\right). \tag{30}$$

The variance and correlation coefficient under this model are shown in Figure 10. The truncated model predicts the variance accurately, although not as well as the Markov chain model for larger a.

4. *Discussion of Correlation Assumptions*

Comparing results for the correlation coefficient κ in Figure 10b, the Markov chain proves to be a far better assumption for larger a. In fact, under the truncated model, the maximum value κ can take is $1/2$ as opposed to the Markov chain model where it approaches 1 in agreement with simulations. This illustrates that, as $a \to \infty$ the higher order correlations $\kappa_2, \kappa_3 ...$ become more important. The truncated model does however provide a slight improvement on the Markov chain assumption in the intermediate region $2 < a < 4$, where the Markov chain model has $\kappa_2 > 0$ when in fact simulation results in Figure 8 show that $\kappa_2 < 0$. As $a \to 0$, the truncated model is qualitatively and quantitatively correct, getting the magnitude of the anti-correlation in this region correct.

V. CALCULATING THE DENSITY FUNCTION

Following the work of McFadden [20, 21], incorporating correlation is achieved through the assumption that the interval densities are linked multiplicatively in the frequency domain with some unknown function of the frequency variable $a_n(s)$. In the previous section, that function is found up to $O(s^2)$ by matching coefficients in the expansions of interval densities. This methodology led to accurate predictions of the interval length variance, in the regions where the interval correlation closure condition was appropriate. The success of this method

demonstrates that the theory is correct up to $O(s^2)$. In this section, by considering poles in the Laplace transform of the density function, we predict the tail of the density function for small a, where $|s| < 1$, and propose further work towards a global expression for the tail of the density function.

A. Persistence

Persistence is the probability $P_e(\tau)$, that there is no zero-crossing by a Gaussian process in the interval $[0, \tau]$. Persistence is related to the PDF $P_0(\tau)$ for the intervals τ between successive crossings by,

$$P_e(\tau) = \int_\tau^\infty P_0(t)\mathrm{d}t.$$

Results by Olla [39] and Eichner *et al* [40] state that, for sufficiently large τ, the form of the tail of $P_0(\tau)$ depends on the auto-correlation function. Specifically, if $\rho(\tau) \sim |\tau|^{-\gamma}$ with $\gamma > 1$, or if it is exponentially bounded such that $\rho(\tau) \sim \exp(-|\tau|^\gamma)$, as is the case for the auto-correlation function considered in this paper, then the asymptotic form of $P_0(\tau)$ does not depend on γ and is given by $P_0(\tau) \sim \exp(-\theta\tau)$. As it also describes the exponential tail of the persistence $P_e(\tau)$, θ is referred to as the persistence parameter. It relates to the length of time until the process changes state and describes how steep the tail of the inter-event PDF is. Previous sections have shown that, as the auto-correlation function becomes more oscillatory, the variance of the inter-event intervals decreases. Equivalently, the PDF will have a steeper tail, and the persistence parameter will increase.

The persistence parameter is examined through the structure of $p_0(s) = \mathcal{L}P_0(\tau)$. The tail of the inter-event density function is $P_0(\tau) \sim \exp(-\theta\tau)$ and the Laplace transform of such an exponential function is

$$\mathcal{L}\left(\exp(-\theta\tau)\right) = \frac{1}{s+\theta}.$$

Hence we expect the Laplace transform of $P_0(\tau)$ to have a simple pole at $s = -\theta$. Consequently the location of the pole in $p_0(s)$ determines the persistence parameter.

B. Uncorrelated Intervals

In the uncorrelated model, $p_n(s) = p_0(s)^{n+1}$, the equation for $p_0(s)$ in terms of $r(s)$ (15) is

$$p_0(s) = \frac{r(s)}{1 - r(s)}$$

which indicates that $p_0(s)$ has a pole at the (negative) value of $s = -\theta$ that solves

$$r(-\theta) - 1 = 0. \tag{31}$$

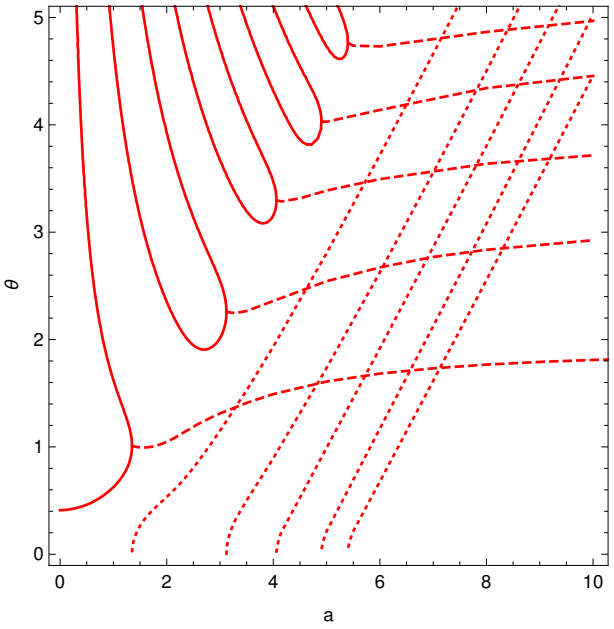

Figure 11. Location of the poles under the uncorrelated assumption given by (31). Real poles are solid lines, complex poles are made up of a real part (dashed line) and imaginary part (dotted line).

The asymptotic form of the inter-event distribution will then be $P_0(\tau) \sim \exp(-\theta\tau)$ where the persistence parameter θ describes the rate of decay.

Due to the oscillatory nature of $\rho'(\tau)$, there are in fact multiple poles of $p_0(s)$. These occur at negative values of $s = -z_j$, where $z_1 < z_2 < z_3...$ are the solutions to

$$\frac{-z}{\pi\bar{r}} \int_0^\infty \frac{\rho'(\tau)\exp(z\tau)}{(1-\rho(\tau)^2)^{1/2}}\mathrm{d}\tau - 1 = 0$$

resulting from inserting equations (10) and (17) into (31).

The topology of the location of the poles in $p_0(s)$, is shown in Figure 11. The real-value locations are established by performing a numerical contour plot of (V B) with a single contour at zero, where the integral is evaluated numerically. Because the complex roots arise from the point at which two real roots coalesce, it is possible to track them from this point.

For a given value of a, taking a vertical slice in Figure 11 gives the multiple roots of (31). For $a < 1.3$ there are infinitely many real-valued roots, the first of which are observed in the plot. At $a \approx 1.35$ the smallest two real roots coalesce, resulting in a complex root, the real and imaginary parts of which are plotted by dashed and dotted lines respectively. More complex roots emerge as further real-valued roots coalesce.

For a given value of a, there exists some $m > 0$ for which the subsequent poles, $z_{m+1}, z_{m+2}....$ are purely real and positive. Furthermore, numerical results show that as $n \to \infty$ the interval between these poles $z_{n+1} - z_n$ approaches π/a so that $z_{n+k} = z_n + k\pi/a$.

Such a spectrum of infinitely many poles in $p_0(s)$ has

not been observed before in the context of the zero-crossing problem.

1. *Calculating the Persistence Parameter For Small a*

The location of the first few poles such that $s = -z_j$, where $z_1 < z_2 < z_3...$, are shown in Figure 13, alongside the simulated value of the persistence parameter θ.

In order to estimate θ, the function $p_0(s)$ can be approximated close to each pole. Expanding $r(s)$ about the location of a pole $s = -z_j$,

$$r(s) = r(-z_j) + r'(-z_j)(s+z_j) + \frac{r''(-z_j)}{2}(s+z_j)^2 + O((s+z_j)^3)$$

with $r(-z_j) = 1$, which upon insertion into (31) gives

$$p_0(s) \approx \frac{-1}{(r'(z_j))(s+z_j)}.$$

Hence the tail of the distribution $P_0(\tau)$ is given by the sum of the relative contribution from each of the poles

$$\lim_{\tau\to\infty} P_0(\tau) \sim \mathcal{L}^{-1}\left(\sum_j \frac{-1}{r'(z_j)(s+z_j)}\right)$$

and the persistence parameter can be determined from a linear fit to

$$\theta = -\frac{\mathrm{d}}{\mathrm{d}\tau}\ln\left|\mathcal{L}^{-1}\left(\sum_j \frac{-1}{r'(z_j)(s+z_j)}\right)\right|. \qquad (32)$$

Figure 12 compares θ obtained from simulations, with that obtained from calculations including only the first term in (32) as well as including the first two terms. For small a including only the first term is sufficient. The magnitude of the least negative pole z_1 coincides with the value of θ obtained from (32). As the location of the second real pole nears the first, its contribution in (32) becomes significant (note that $r'(-z_1)$ and $r'(-z_2)$ are necessarily of opposite sign) creating logarithmic modifications to the tail of the PDF which persist even for $\tau/\langle\tau\rangle > 1$. The effect of these adjustments is that, when including the second term in calculations, the persistence parameter is *reduced* from that value predicted by the first regarded in isolation, giving an improved estimate.

The first two real roots merge at $a \approx 1.34$, whereupon the root becomes complex, the real part being shown in Figure 13 by the dashed curve, the imaginary part by the dotted curve. When determining θ under (32), the value of $\mathrm{Re}(z_1)$, places an upper bound on the value calculated for θ. Figure 13 shows that for $a > 1.6$ the simulated value of θ exceeds $\mathrm{Re}(z_1)$ and is increasing at a far greater rate. The simulated values for θ are much higher, and hence the decay of the tail much faster, than this model will predict. In this region, the correlations between intervals must be incorporated into the model.

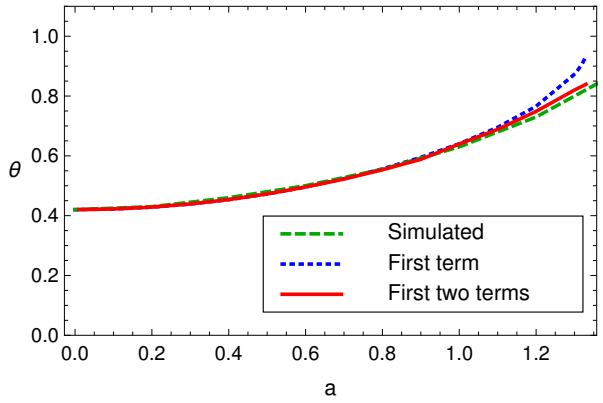

Figure 12. The persistence parameter θ, from simulations (green dashed), from considering only the first term in (32) (blue) and from considering the first two terms in (32) (red).

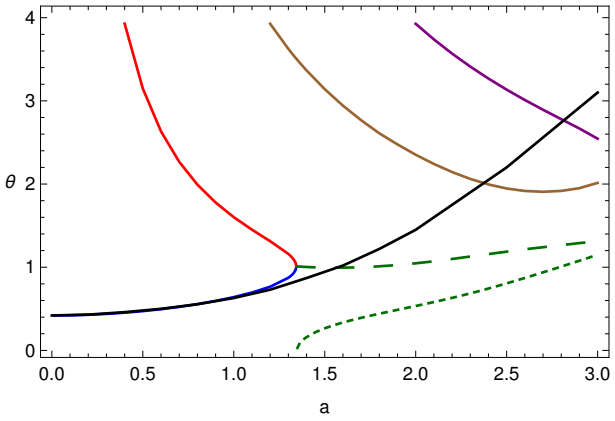

Figure 13. The real (solid lines) and complex (real part: dashed line, imaginary part: dotted line) poles of (31), as well as the simulated value of θ (solid black line)

C. Correlated Intervals

In section IV B the variance and correlation coefficients were effectively modelled through the introduction of the function $a_n(s)$ into the assumed model so that:

$$p_n(s) = a_n(s)p_0^{n+1}(s).$$

Using the fact that $p_n(s)$ is a moment generating function, $a_n(s)$ was determined up to $O(s^2)$ under a suitable closure condition for the correlation coefficients. Considering $a < 3$ then, the truncated correlation model is appropriate, for which solving the quadratic (28) in favour of $p_0(s)$, gives

$$p_0(s) = \frac{(2r(s)-1) \pm \left(1 - 4\kappa\sigma^2 s^2 r(s)\right)^{1/2}}{-2\left(r(s) - 1 + \kappa\sigma^2 s^2\right)}.$$

Taking the '+' solution, poles of $p_0(s)$ occurs where the denominator of vanishes when $s \to -\theta$, which now becomes the solution of

$$r(-\theta) - 1 = -\kappa\sigma^2\theta^2. \qquad (33)$$

Note that this is not a linear perturbation of the uncorrelated assumption result in (31) (the correlation coefficient features explicitly and coupled with σ^2 but retrieves it if $\kappa = 0$.

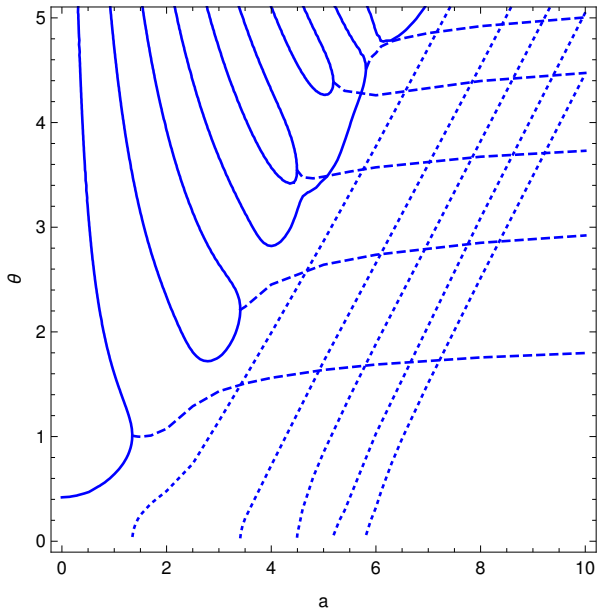

(a) The poles in the correlated intervals case given by equation (33). Real poles (solid lines) coalesce to form complex poles made up of a real part (dashed line) and imaginary part (dotted line).

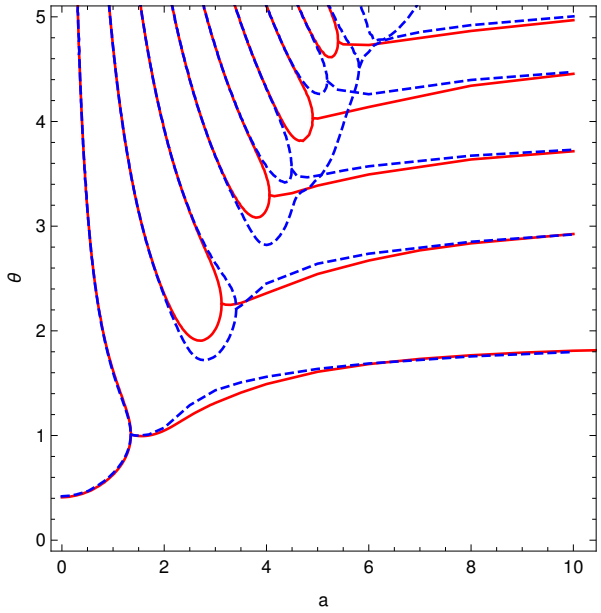

(b) The real part of poles in the correlated case (dashed), equation (33), and the uncorrelated case (solid), equation (31)).

Figure 14. The poles in the Laplace transform of the interval density function, in the correlated intervals case and in comparison to the uncorrelated.

Figure 14 shows the topology of the poles for the correlated case, and in comparison to the uncorrelated case. The correlated case displays very similar results to the uncorrelated case, but the way in which the real-valued poles coalesce is slightly different. As $\sigma^2 \sim \left(56/a^7\right)^{1/2}$ for $a \gg 1$ (25) and $|\kappa| \leq 1$ the roots of the correlated case (33) approach those of the uncorrelated case (31). This can be seen in the Figure 14b; although the structure is different when they first emerge, with increasing a the complex roots tend to the same value as found in the uncorrelated case.

Again, the function $p_0(s)$ can be approximated close to each pole. Expanding $r(s)$ about the location of a pole $s = -z_j$,

$$r(s) = r(-z_j) + r'(-z_j)(s + z_j) + \frac{r''(-z_j)}{2}(s + z_j)^2 + O((s + z_j)^3)$$

with $r(-z_j) = 1 + \kappa\sigma^2 s^2$, which upon insertion into (V C) gives

$$p_0(s) \approx \frac{2\kappa\sigma^2 z_j^2 - 1}{(r'(z_j) + 2\kappa\sigma^2 z_j)(s + z_j)}.$$

The persistence parameter can then be determined from a linear fit to

$$\theta = -\frac{\mathrm{d}}{\mathrm{d}\tau} \ln \left| \mathcal{L}^{-1} \left(\sum_j \frac{2\kappa\sigma^2 z_j^2 - 1}{f'(z_j)(s + z_j)} \right) \right|$$

with $f(s) = r(s) - \kappa\sigma^2 s^2$.

Estimating θ in this way does not improve on the uncorrelated result because $\kappa\sigma^2 \ll 1$. Again, $\mathrm{Re}(z_1)$ places an upper bound on the value calculated for θ. It is clear from Figure 14 that the truncated correlated model does not significantly improve upon the uncorrelated one. There is also no significant improvement under the Markov chain assumption. In both cases, the problem lies in the expansion of $a_n(s)$.

Using polynomial expansions to locate poles in $p_0(s)$ is only appropriate in the region where the s expansion for $a_0(s)$ applies. Under both closure conditions $a_0(s)$ is approximated as:

$$a_n(s) = 1 + s^2\sigma^2\kappa f(n, \kappa) + o(s^2)$$

for some function f such that $f(0, \kappa) = 0$ and $f(n, \kappa)$ is positive when $n \geq 0$ and $0 < \kappa < 1$. As $a \to \infty$, $\sigma^2\kappa \to 0$, which means that the $O(s^2)$ expansion of $a_n(s) \to 1$ and hence the correlated intervals model approaches the uncorrelated intervals model under both closure conditions. Simulation results show that, as $a \to \infty$, κ has far greater influence than this model would suggest. The PDF becomes more singular so that $P_n(\tau)$ tends towards a delta-function located at the mean interval spacing $(n + 1)\langle\tau\rangle$.

D. Transitional Model

The above model for $p_n(s)$ could never describe a delta function and so, in the situation when $a \to \infty$,

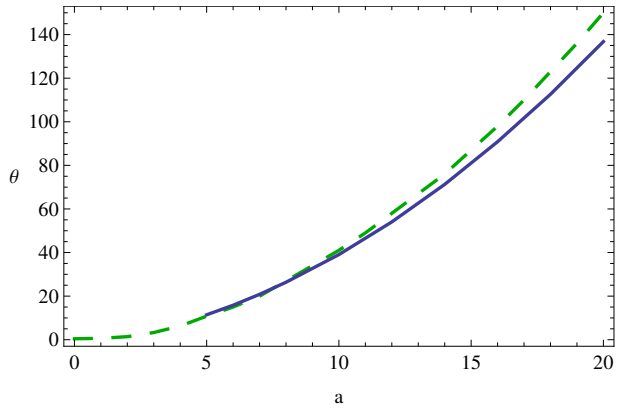

Figure 15. The persistence parameter from simulations (green dashed) and estimated for $a \geq 5$ via (35) and (36) with $\mu = 4.5$ (solid blue)

an adapted model is designed to account for this:

$$p_n(s) = \hat{p}_0((1-\kappa)^\mu s)^{n+1} \exp\left(-(n+1)\kappa\langle\tau\rangle s\right)$$

for some $\mu > 0$ and where $\hat{p}_0(s)$ satisfies the uncorrelated model which was shown to be sufficient for smaller a:

$$\hat{p}_n(s) = \hat{p}_0(s)^{n+1}. \tag{34}$$

When $\kappa = 0$ this model has the same structure as the uncorrelated model (34). As $a \to \infty$, $\kappa \to 1$ and

$$p_n(s) = \exp\left(-(n+1)\langle\tau\rangle s\right)$$

which is the Laplace transform of a delta-function located at the mean interval spacing.

Essentially this model provides a transition from the PDF being a solution to the uncorrelated model (valid for small a), to the PDF being a delta function at the mean interval length (valid for infinitely large a). As $a \to \infty$, the PDF suggested by (34) is compressed and the influence of the delta-function increases.

For large a the asymptotic result for κ (26) is

$$\kappa \sim \frac{1-\alpha}{1+\alpha} \sim \frac{1-\left(\frac{8}{7a}\right)^{1/2}}{1+\left(\frac{8}{7a}\right)^{1/2}}$$

which is a good approximation when $a \geq 5$. In this region the poles of $p_0(s)$ then occur at the poles of $\hat{p}_0((1-\kappa)^\mu s)$ which are given by (31) as $s = -z_j$, the solution to

$$r(-(1-\kappa)^\mu z_j) - 1 = 0. \tag{35}$$

The persistence parameter is then estimated as

$$\theta = \mathrm{Re}(z_1) \tag{36}$$

where z_1 is the smallest root.

Figure 15 shows the persistence parameter from simulations, and estimated via (35) and (36) with $\mu = 4.5$, for the region $a \geq 5$ where the asymptotic result for κ is accurate. The transitional model captures the rate of increase in the persistence parameter as the PDF tends towards a delta function for large a.

E. Future Work

In this section, by considering poles in the Laplace transform of the density function, we were also able to accurately predict the tail of the density function for small a, where $|s| < 1$. However, we were not able to locate poles in $p_0(s)$ where $|s| > 1$. Doing so would require the global form of $a_n(s)$.

One plausible model for tackling this problem would be to renormalise the function so that

$$a_n(s) = 1 \pm \kappa\sigma^2 s^2 \exp\left[-|f(s)|\right] \tag{37}$$

with $f(0) = 0$. Such a model would incorporate terms of the form

$$\langle\tau_i\tau_{i+j}\tau_{i+j+k}\ldots\rangle. \tag{38}$$

The related higher order correlations $\kappa_{i,j,k,\ldots}$ must all tend towards unity as determinism is approached when $a \to \infty$. In addition, further analysis of the persistence would be helped with more accurate simulations extending further into the tail of the distribution. Because intervals of these lengths are extremely rare, this would require a great deal more time and computational power.

VI. SUMMARY

The model presented in this paper explores systematically the changes that occur between a random signal and a deterministic one. Study of the effects of oscillation in the auto-correlation function has revealed a sliding scale of regularity in the zero-crossings of Gaussian processes. For both the power-law auto-correlation function and the Gaussian limit case, more oscillations in the auto-correlation function mean zero-crossings occur at more regular intervals. As zero-crossings become more regular, the random intervals between them have reduced variance and a more localised, tending to singular, probability density function. This will prove useful for modelling any process upon which there is a periodic variation. For example, the diurnal and annual variations implicit in weather, climate, traffic, energy demand, sleep patterns, and many more, or in analysis of signals which result from some combination of periodicity and random noise such as in interferometry or tomography.

This work demonstrates that the entire structure of the auto-correlation function of the random process is the principal cause for the rich phenomenology exhibited by the derived process of the inter-event intervals. In particular, the oscillatory behaviour in the auto-correlation function is a way of punctuating a random process by deterministic features. The way these become manifested is subtle, first involving an interplay between the characteristic scale-sizes associated with the higher order statistics, but eventually cascading throughout the entire process as it becomes progressively more correlated. Divining how these scale-sizes emerge from the properties of the

auto-correlation function remains an area for fruitful investigation.

[1] S N Majumdar, C Sire, A J Bray, and S J Cornell, "Nontrivial exponent for simple diffusion," Phys. Rev. Lett. **77**, 2867–2870 (1996).

[2] W B Davenport, Jr and W L Root, *An Introduction to the Theory of Random Signals and Noise*, ieee press ed. (IEEE Press, 1987).

[3] RG Bachu, S Kopparthi, B Adapa, and Buket D Barkana, "Voiced/unvoiced decision for speech signals based on zero-crossing rate and energy," in *Advanced Techniques in Computing Sciences and Software Engineering* (Springer, 2010) pp. 279–282.

[4] P E William and M W Hoffman, "Identification of bearing faults using time domain zero-crossings," Mechanical systems and signal processing **25**, 3078–3088 (2011).

[5] R Wiley, "Approximate FM demodulation using zero crossings," Communications, IEEE Transactions on **29**, 1061 – 1065 (1981).

[6] G. Lindgren, "Wave analysis by slepian models," Probabilistic Engineering Mechanics **15**, 49 – 57 (2000).

[7] Georg Lindgren, "Horseshoe-like patterns in first-order 3d random gauss-lagrange waves with directional spreading," Waves in Random and Complex Media **25**, 729–745 (2015).

[8] J D Salas, C Chung, and A Cancelliere, "Correlations and crossing rates of periodic-stochastic hydrologic processes," Journal of Hydrologic Engineering **10**, 278–287 (2005).

[9] P J Edwards and R B Hurst, "Level-crossing statistics of the horizontal wind speed in the planetary surface boundary layer," Chaos: An Interdisciplinary Journal of Nonlinear Science **11**, 611–618 (2001).

[10] P Douglas, "The persistence exponent of DNA," Biophysical Chemistry **110**, 59 – 72 (2004).

[11] M-C Wu, M-C Huang, H-C Yu, and T C Chiang, "Phase distribution and phase correlation of financial time series," Phys. Rev. E **73**, 016118 (2006).

[12] M Constantin and S Das Sarma, "Volatility, persistence, and survival in financial markets," Phys. Rev. E **72**, 051106 (2005).

[13] P H Brill, "An embedded level crossing technique for dams and queues," Journal of Applied Probability , 174–186 (1979).

[14] I Rychlik, "On some reliability applications of Rice's formula for the intensity of level crossings," Extremes **3**, 331–348 (2000).

[15] G Lindgren, "Wave-length and amplitude in gaussian noise," Advances in Applied Probability **4**, pp. 81–108 (1972).

[16] T Malevich, "Asymptotic normality of the number of crossings of level zero by a gaussian process," Theory of Probability and Its Applications **14**, 287–295 (1969).

[17] I Blake and W Lindsey, "Level-crossing problems for random processes," Information Theory, IEEE Transactions on **19**, 295 – 315 (1973).

[18] E Wong, "Some results concerning the zero-crossings of gaussian noise," SIAM Journal on Applied Mathematics **14**, 1246–1254 (1966).

[19] L R M Wilson, K I Hopcraft, and E Jakeman, "The influence of oscillatory correlation on the zero crossings of gaussian processes," in *Vulnerability, Uncertainty, and Risk: Quantification, Mitigation, and Management*, edited by M Beer, S-K Au, and J W Hall (ASCE, 2014) pp. 1856–1865.

[20] J A McFadden, "The axis-crossing intervals of random functions," IRE Trans. Inform. Theory **IT-2**, 146 (1956).

[21] J A McFadden, "The axis-crossing intervals of random functions-II," IRE Trans. Inform. Theory **IT-4**, 14 (1958).

[22] D M Gordon, "Control without hierarchy," Nature **446**, 143–143 (2007).

[23] E Ziff and I Rosenfield, "Evolving evolution," The New York Review of Books **53** (2006).

[24] J Gerhart, M Kirschner, and E S Moderbacher, *Cells, embryos, and evolution: Toward a cellular and developmental understanding of phenotypic variation and evolutionary adaptability* (Blackwell Science Malden, 1997).

[25] M Mitchell, *Complexity: A guided tour* (Oxford University Press, 2009).

[26] N Wiener, "Generalized harmonic analysis," Acta mathematica **55**, 117–258 (1930).

[27] A Khintchine, "Korrelationstheorie der stationären stochastischen prozesse," Mathematische Annalen **109**, 604–615 (1934).

[28] E Jakeman and K D Ridley, *Modeling Fluctuations in Scattered Waves*, 1st ed. (Taylor and Francis, 2006).

[29] R Leadbetter, G Lindgren, and H Rootzén, *Extremes and related properties of random sequences and processes*, Springer Series in Statistics (Springer-Verlag, 1983).

[30] M Abramowitz and I A Stegun, *Handbook of Mathematical Functions: with Formulas, Graphs, and Mathematical Tables*, Dover Books on Mathematics (Dover Publications, 2012).

[31] S O Rice, "Mathematical analysis of random noise," in *Selected Papers on Noise and Stochastic Processes*, edited by N. Wax (Dover Publications, 1954).

[32] U Fano, "Ionization yield of radiations. ii. the fluctuations of the number of ions," Phys. Rev. **72**, 26–29 (1947).

[33] U T Eden and M A Kramer, "Drawing inferences from fano factor calculations," Journal of neuroscience methods **190**, 149–152 (2010).

[34] C. W. J. Beenakker, M. Patra, and P. W. Brouwer, "Photonic excess noise and wave localization," Phys. Rev. A **61**, 051801 (2000).

[35] H Steinberg, P M. Schultheiss, C A Wogrin, and F Zweig, "Short-time frequency measurement of narrow-band random signals by means of a zero counting process," Journal of Applied Physics **26**, 195 –201 (1955).

[36] E. Jakeman and K. D. Ridley, "Signal processing analog of phase screen scattering," J. Opt. Soc. Am. A **15**, 1149–1159 (1998).

[37] I.G. Usoskin and K. Mursula, "Long-term solar cycle evolution: Review of recent developments," Solar Physics **218**, 319–343 (2003).

[38] J H Van Vleck and D Middleton, "The spectrum of clipped noise," Proceedings of the IEEE **54**, 2–19 (1966).

[39] P Olla, "Return times for stochastic processes with

power-law scaling," Phys. Rev. E **76**, 011122 (2007).
[40] J F Eichner, J W Kantelhardt, A Bunde, and S Havlin, "Statistics of return intervals in long-term correlated records," Phys. Rev. E **75**, 011128 (2007).